

Electronic states in a quantum lens

Arezky H. Rodríguez^(a), C. Trallero-Giner^(a), S.E. Ulloa^(b) and J. Marín-Antuña^(a)

^(a) *Department of Theoretical Physics, University of Havana, 10400,
Havana, Cuba*

^(b) *Department of Physics and Astronomy and CMSS Program, Ohio
University, Athens, Ohio 45701-2979
(18 July 2000)*

Abstract

We present a model to find analytically the electronic states in self-assembled quantum dots with a truncated spherical cap ('lens') geometry. A conformal analytical image is designed to map the quantum dot boundary into a dot with semi-spherical shape. The Hamiltonian for a carrier confined in the quantum lens is correspondingly mapped into an equivalent operator and its eigenvalues and eigenfunctions for the corresponding Dirichlet problem are analyzed. A modified Rayleigh-Schrödinger perturbation theory is presented to obtain analytical expressions for the energy levels and wavefunctions as a function of the spherical cap height b and radius a of the circular cross section. Calculations for a hard wall confinement potential are presented, and the effect of decreasing symmetry on the energy values and eigenfunctions of the lens-shape quantum dot is studied. As the degeneracies of a semi-circular geometry are broken for $b \neq a$, our perturbation approach allows tracking of the split states. Energy states and electronic wavefunctions with $m = 0$ present the most pronounced influence on the reduction of the lens height. The analytical expressions presented here can be used to better parameterize the states in realistic self-assembled quantum dots.

PACS99: 73.61.-r, 73.20.Dx, 03.65.Ge, 78.30.Fs

Typeset using REVTeX

I. INTRODUCTION

Quantum dots obtained by interrupted growth in strained semiconductor interfaces are currently under intense study by many experimental and theoretical groups.¹ These ‘self-assembled’ quantum dots are mostly dislocation free, coherent islands of deposited material on the surface of a different semiconductor. The lattice mismatch from one semiconductor to the other forces the segregation of material whenever the epitaxial growth exceeds a critical layer thickness, resulting in the growth of these so-called Stranski-Krastanov islands.² Deposition of material past a critical thickness, which depends on the two materials used, results in large arrays of small islands with a rather narrow size distribution (with size variations well under 10%), and typically arranged randomly on the plane (although avoiding overlapping islands, for the most part).¹ More recently, some groups are working at producing in-plane ordering of islands following different approaches, including ‘nucleation site engineering’ to favor certain locations for self-assembled dot growth.³ These self-assembled quantum dots have, for the most part, a large area-to-height aspect ratio. In the case of InAs islands grown on a GaAs surface, the in-plane diameters are typically less than 30 nm, while their heights are below 10 nm.⁴ Although not without some controversy, it is generally believed that the InAs quantum dots on GaAs are shaped like a ‘lens’, characterized by a spherical cap shape with circular cross section. Upon optical or other mechanisms of carrier injection, both electrons or holes have bound well-confined states inside these dots.

In fact, optical experiments on self-assembled dots demonstrate that these structures provide strong carrier confinement, as decreasing dot size produces strong blue-shift of the extremely-narrow luminescence peaks in *isolated* dots.^{5–9} Confinement effects have also been shown to appear in magneto-capacitance and infrared absorption experiments by several groups.^{10–13} Clear evidence of electronic shell states and their different degeneracies has been reported recently,¹⁴ and novel applications such as storage of photoluminescence signals was demonstrated recently in gate-activated ‘optical memories.’¹⁵

Simplifying the symmetry of the lens as a two-dimensional harmonic oscillator has been suggested to characterize the level structure for charge carriers in the dots, and this has proven useful in the interpretation of experiments.¹⁶ Nevertheless, as we will show here, a lens geometry has quite a different level structure and wavefunctions with subtle symmetries which might be seen in experiments. For example, we find that as the height of the cap or lens decreases, there is a larger shift of the wavefunction towards the plane of the lens (in comparison with the situation in a semi-spherical geometry). This shift becomes stronger for ‘flatter’ lenses, and may even give rise to deconfinement of the state towards the substrate, for finite confinement potential, changing significantly the oscillator strength of electron-hole transitions, for example.¹⁷ However, even before that occurs, the smaller height lens geometries exhibit a different level structure than the harmonic oscillator, as we show below. This structure may give rise to different Pauli blocking effects and transition rules, topics which are the subject of interest in recent experiments.¹⁸

In this paper we rigorously show that a complete set of wavefunctions can be generated with the correct lens symmetry to describe the physical properties given by the differential equation of interest. For the sake of simplicity, we have applied our calculation here to the single-particle Schrödinger equation. The incorporation of non-parabolic band dispersion or many-particle interactions is straightforward (if only a bit cumbersome). Notice that while

our calculation provides an analytical approach to the understanding of electronic states in these structures, it also provides an interesting example of a generalization of perturbation theory for the conformally-mapped differential operator arising from the Schrödinger equation in the material. Since the conformal transformation used to map the lens into the semi-spherical geometry is non-trivial, the resulting differential equation in the transformed space reflects that complexity. Fortunately, our perturbation approach is robust for the identified small parameter of the problem, as we will show.

The remainder of the paper is structured as follows: in section II we introduce the problem of the spherical cap geometry, its semi-spherical limit, and the conformal map which connects the two shapes. In that section, we also describe the perturbation approach needed to carry out the solution of the appropriately mapped Schrödinger operator, and explore the orthonormalization conditions of the basis used in the description of the general problem. In section III we present some examples of the eigenstates for varying lens size, and analyze their angular and radial distribution functions. Section IV presents some discussions and conclusions, while the appendix contains details of the expansion described in section II.

II. DIRICHLET PROBLEM FOR A QUANTUM LENS: CONFORMAL MAPPING

The shape of the quantum lens in real \mathbf{r} -space is shown in Fig. 1(a). $R_3(a, b)$ denotes the domain of the lens with boundary in \mathbf{r} -space given by a spherical cap of height b and circular cross section with radius a . Assuming a carrier Hamiltonian model with isotropic band and effective mass m^* , the eigenvalue problem for a particle confined in the lens is described by the operator

$$\hat{H} = -\frac{\hbar^2}{2m^*}\nabla_{\mathbf{r}}^2 \quad ; \quad \mathbf{r} \in R_3(a, b), \quad (1)$$

obeying the Dirichlet boundary condition $\psi = 0$ for $\mathbf{r} \in L_3(a, b)$. $L_3(a, b)$ is the boundary of the $R_3(a, b)$ domain. The operator (1) presents axial symmetry and all functions defined on $R_3(a, b)$ have the property $\phi(\varphi) = \phi(\varphi + 2\pi)$, where φ is the axial angle. Hence, the solution of (1) can be written as

$$\psi(\mathbf{r}) = f(\boldsymbol{\rho}) \frac{e^{i m \varphi}}{\sqrt{2\pi}} \quad ; \quad m = 0, \pm 1, \pm 2, \dots, \quad (2)$$

where $\boldsymbol{\rho}$ is a 2D vector. Correspondingly, the operator (1) is transformed into an eigenvalue problem for $f(\boldsymbol{\rho})$,

$$\left[\nabla_{\boldsymbol{\rho}}^2 + \left(k_o^2 - \frac{m^2 - 1/4}{\rho^2 \sin^2 \theta} \right) \right] f(\boldsymbol{\rho}) = 0 \quad ; \quad \boldsymbol{\rho} \in R_2(a, b), \quad (3)$$

where $k_o^2 = 2m^*E/\hbar^2$, E is the energy of the eigenfunction $f(\boldsymbol{\rho})$, θ is the polar angle, and $R_2(a, b)$ is the 2D domain with boundary $L_2(a, b)$ in the $\boldsymbol{\rho}$ -space shown in Fig. 1(b). The Hilbert space where the operator (3) is defined corresponds to the set of functions $f(\boldsymbol{\rho}) \in R_2(a, b)$ with boundary condition $f(\boldsymbol{\rho}) = 0$ on $L_2(a, b)$.

A. Semi-spherical quantum dot

For the case of $b = a$, the lens shape of Fig. 1(a) has semi-spherical symmetry. Hence, the Dirichlet problem in (3) reduces to the conditions $f(a, \theta) = 0$, and $f(\rho, \pi/2) = 0$. The set $\{f_i\}$ of eigenfunctions of (3) on the R_2 domain forms an orthonormal basis with functions which in polar coordinates are given by products of the associate Legendre polynomials and Bessel functions,

$$f_{n,l}^{(0)}(\rho, \theta) = \sqrt{\sin \theta} \frac{P_l^{|m|}(\cos \theta)}{N_{l,m}} \frac{J_{l+\frac{1}{2}}(\frac{\mu_n^{(l)}}{a}\rho)}{N_B}, \quad (4)$$

with $l = 0, 1, 2, \dots$, and the condition $-l \leq m \leq l$. The normalization constants $N_{l,m}$ and N_B are as usual given by

$$N_{l,m} = \sqrt{\frac{1}{2l+1} \frac{(l+|m|)!}{(l-|m|)!}} \quad ; \quad N_B = \frac{a}{\sqrt{2}} J'_{l+\frac{1}{2}}(\mu_n^{(l)}), \quad (5)$$

where J'_q is the derivative of the Bessel function J_q , and $\mu_n^{(p)}$ is the n -th zero, $J_{p+\frac{1}{2}}(\mu_n^{(p)}) = 0$. The eigenvalues are given by $E_{n,l} = \hbar^2 (\mu_n^{(l)})^2 / (2m^*a^2)$, and the boundary condition $f^{(0)}(\rho, \theta = \pi/2) = 0$ restricts the values of the quantum numbers l and m to fulfill the condition $|l - m| = \text{odd}$. According to this condition, the degeneracy of states $f_{n,l}^{(0)}$ for a given energy $E_{n,l}$ is equal to l and the ground state corresponds to $l = 1$, $m = 0$, and $n = 1$.

B. Quantum lens

The quantum dot with lens shape corresponds to the more general case when $b < a$. Here, we need to fulfill Eq. (3) with the Dirichlet condition over the boundary $L_2(a, b)$. The wavefunctions $f_{n,l}^{(0)}$ given by (4) are not solution for the general case, because the problem has no longer the semi-circular symmetry in θ . The energy number n and angular momentum l are clearly no longer good quantum numbers when $b \neq a$ and the m -degeneracy is broken. To obtain an analytical solution of the problem (3) it is convenient to make a conformal mapping to the circular cap with domain $R_2(a, a)$ and boundary $L_2(a, a)$. The mapping enables us to solve the Dirichlet problem for the operator given by (3) in a Hilbert space where an orthonormal basis $\{f_i\}$ is known. We transform the quantum lens domain and boundary into a dot with semi-spherical shape, so that the circular cap defined by the domain $\mathcal{Z} = x - iz \in R_2(a, b)$, transforms into the semi-circular domain $\mathcal{W} = u - iv \in R_2(a, a)$. This is accomplished by the transformation (see Fig. 1(b))

$$\mathcal{W}(\mathcal{Z}) = \frac{2a}{1 + \left(\frac{a - \mathcal{Z}}{a + \mathcal{Z}}\right)^\alpha} - a \quad ; \quad \alpha = \frac{\pi/4}{\arctan(b/a)}. \quad (6)$$

In the complex plane \mathcal{W} , we have the parameter equations: $u = \rho \sin \theta$, $v = \rho \cos \theta$, $0 < \rho < a$, $0 < \theta < \pi/2$. The eigenvalue problem (3) is thus transformed by this conformal mapping into the problem

$$\nabla_{(u,v)}^2 F(u,v) + \mathcal{J}_\alpha(u,v) \left(k^2 - \frac{m^2 - 1/4}{\mathcal{X}_\alpha^2(u,v)} \right) F(u,v) = 0 ; (u,v) \in R_2(a,a), \quad (7)$$

with the boundary condition,

$$F(u,v) |_{(u,v) \in L_2(a,a)} = 0. \quad (8)$$

The functions $\mathcal{J}_\alpha(u,v) = \left| \frac{d\mathcal{Z}}{dW} \right|^2$ (the Jacobian) and $\mathcal{J}_\alpha/\mathcal{X}_\alpha^2$ are given in the Appendix, and are mathematical objects which contain the information of the lens geometry, where the subscript α is given in (6). It should be noted that $\alpha \geq 1$, since $b \leq a$, and for $\alpha = 1$ the Jacobian \mathcal{J}_α reduces to 1, while $\mathcal{J}_\alpha/\mathcal{X}_\alpha^2$ reduces to $1/u^2 = 1/(\rho \sin \theta)^2$.

The Hilbert space on which the operator (7) is defined must fulfill the Dirichlet boundary conditions indicated in (8). A set of functions that fulfill these boundary conditions are the functions $f_{n,l}^{(0)}$ given in (4), and represent a complete set of orthonormal eigenfunctions for the operator in (7). The solution $F(u,v)$ for a given m can be expanded in term of the set $\{f_{n,l}^{(0)}\}$ such that

$$F = \sum_{n,l} C_{n,l} f_{n,l}^{(0)}(\boldsymbol{\rho}), \quad (9)$$

where $\boldsymbol{\rho} = (\rho, \theta)$ is here the parameterization of (u,v) , and the functions $f_{n,l}^{(0)}$ are restricted to the condition $|l - m| = \text{odd}$. The coefficients $C_{n,l}$ have to be determined to satisfy the full operator; a perturbation procedure to accomplish this is described in section IID below.

C. Orthogonality and completeness

Equation (7) can be cast in operator form as

$$\hat{\mathbf{K}} F = \mathcal{J}_\alpha k^2 F, \quad (10)$$

where $\hat{\mathbf{K}}$ involves the Laplace operator, $-\nabla_{(u,v)}^2$, and the term $(m^2 - 1/4)\mathcal{J}_\alpha/\mathcal{X}_\alpha^2(u,v)$. Equation (10) is an eigenvalue problem for the dimensionless energies $k_N^2(m)$, where N is a generic label for the different eigenstates F_N of (10). Let us now suppose that N and M correspond to different eigenvalues of (10). From the above equation it follows that

$$F_M^* \hat{\mathbf{K}} F_N - F_N \hat{\mathbf{K}}^* F_M^* = \mathcal{J}_\alpha (k_N^2 - k_M^2) F_M^* F_N. \quad (11)$$

Making the integration over $\boldsymbol{\rho}(u,v)$ in the $R_2(a,a)$ domain, we obtain that

$$\int_{R_2(a,a)} \left[-F_M^* \nabla_{(u,v)}^2 F_N + F_N \nabla_{(u,v)}^2 F_M^* \right] d^2 \rho = (k_N^2 - k_M^2) \int_{R_2(a,a)} F_M^* F_N \mathcal{J}_\alpha d^2 \rho. \quad (12)$$

Integration by parts gives us

$$(k_N^2 - k_M^2) \int_{R_2(a,a)} \mathcal{J}_\alpha F_M^* F_N d^2 \rho = (F_N \nabla F_M^* - F_M^* \nabla F_N) |_{(u,v) \in L_2(a,a)}, \quad (13)$$

which due to the boundary condition (8), it is reduced to

$$(k_N^2 - k_M^2) \int_{R_2(a,a)} \mathcal{J}_\alpha F_M^* F_N d^2\rho = 0. \quad (14)$$

For $N \neq M$, condition (14) represents the orthogonality property of the eigenfunction set $\{F_N\}$, where \mathcal{J}_α is clearly the *weighting factor* of the eigenproblem (7). Moreover, the operator $\hat{\mathbf{K}}$ is Hermitian, ensuring that the solution of the present problem is described by means of a complete orthonormal basis of eigenfunctions $\{F_N\}$ obeying the condition

$$\int_{R_2(a,a)} \mathcal{J}_\alpha F_M^* F_N d^2\rho = \delta_{N,M}. \quad (15)$$

D. Perturbation theory

The coefficients $C_{n,l}$ in (9) and the eigenvalues k^2 can be obtained by perturbation theory if $b \approx a$ ($\alpha \rightarrow 1$). In this case, the lens cap represents a perturbation from the semi-spherical geometry. In other words, the operator (7) can be rewritten in the form

$$(H_o + H_p) F(u, v) = 0, \quad (16)$$

with

$$H_o(u, v) = \nabla_{(u,v)}^2 + \left(k^2 - \frac{m^2 - 1/4}{u^2} \right), \quad (17)$$

$$H_p(u, v) = k^2 \left(\mathcal{J}_\alpha(u, v) - 1 \right) - (m^2 - 1/4) \left(\frac{\mathcal{J}_\alpha(u, v)}{\mathcal{X}_\alpha^2(u, v)} - \frac{1}{u^2} \right). \quad (18)$$

The operator H_p vanishes when $\alpha \rightarrow 1$ ($b \rightarrow a$) and it can be considered as a small perturbation operator, when the height b is close to the radius a . The set $\{f_{n,l}^{(0)}\}$ given by Eq. (4) are the eigenfunctions of the Hamiltonian H_o in the \mathcal{W} -space and form an orthonormal basis on the $R_2(a, a)$ domain. In order to find the solution of (16) as a function of the ratio b/a , we will develop a modified Rayleigh-Schrödinger perturbation theory. We note that the perturbation Hamiltonian H_p depends on the eigenvalue k^2 , and as such requires a somewhat different approach. Substituting Eq. (9) in (16) we obtain

$$\begin{aligned} & \left[(k^2 - k_o^2) + \langle n, l | H_p(k^2) | n, l \rangle \right] C_{n,l} + \\ & + \sum_{n', l' \neq n, l} \langle n, l | H_p(k^2) | n', l' \rangle C_{n', l'} = 0. \end{aligned} \quad (19)$$

The states of H_o are degenerate on the quantum number m . Nevertheless, according to (2),

$$\langle n, l, m | H_p | n', l', m' \rangle = \langle n, l | H_p | n', l' \rangle \delta_{m, m'}, \quad (20)$$

so that the matrix elements are diagonal on m and we can develop a perturbation theory in the absence of degeneracy. We represent the coefficients $C_{n,l}$ and its eigenvalues k^2 in a

power series of the small parameter $\lambda = \alpha^{-1} - 1$ (which arises naturally from the expressions in the Appendix). We obtain up to first order in λ an expression for the wavefunctions given by

$$F_{N,m}(\rho, \theta) = f_{n,l}^{(0)}(\rho, \theta) + \lambda \left[-\frac{1}{2} \left\langle n, l \left| \left(\frac{\partial \mathcal{J}_\alpha}{\partial \lambda} \right)_{\lambda=0} \right| n, l \right\rangle f_{n,l}^{(0)}(\rho, \theta) + \sum_{n', l' \neq n, l} f_{n', l'}^{(0)}(\rho, \theta) \times \frac{1}{k_o^2(n', l') - k_o^2(n, l)} \times \left\langle n', l' \left| k_o^2(n, l) \left(\frac{\partial \mathcal{J}_\alpha}{\partial \lambda} \right)_{\lambda=0} - (m^2 - 1/4) \frac{\partial}{\partial \lambda} \left(\frac{\mathcal{J}_\alpha}{\mathcal{X}_\alpha^2} \right)_{\lambda=0} \right| n, l \right\rangle \right]. \quad (21)$$

We find for the eigenvalues up to second order, that

$$k^2(N, m) = k_o^2(n, l) + \lambda k_1^2(N, m) + \lambda^2 k_2^2(N, m), \quad (22)$$

where

$$k_1^2(N, m) = - \left\langle n, l \left| k_o^2(n, l) \left(\frac{\partial \mathcal{J}_\alpha}{\partial \lambda} \right)_{\lambda=0} - (m^2 - 1/4) \frac{\partial}{\partial \lambda} \left(\frac{\mathcal{J}_\alpha}{\mathcal{X}_\alpha^2} \right)_{\lambda=0} \right| n, l \right\rangle, \quad (23)$$

$$k_2^2(N, m) = - \sum_{n', l' \neq n, l} \frac{\left\langle n', l' \left| k_o^2(n, l) \left(\frac{\partial \mathcal{J}_\alpha}{\partial \lambda} \right)_{\lambda=0} - (m^2 - 1/4) \frac{\partial}{\partial \lambda} \left(\frac{\mathcal{J}_\alpha}{\mathcal{X}_\alpha^2} \right)_{\lambda=0} \right| n, l \right\rangle^2}{k_o^2(n', l') - k_o^2(n, l)} - \frac{1}{2} \left\langle n, l \left| k_1^2(N, m) \left(\frac{\partial \mathcal{J}_\alpha}{\partial \lambda} \right)_{\lambda=0} + k_o^2(n, l) \left(\frac{\partial^2 \mathcal{J}_\alpha}{\partial \lambda^2} \right)_{\lambda=0} - (m^2 - 1/4) \frac{\partial^2}{\partial \lambda^2} \left(\frac{\mathcal{J}_\alpha}{\mathcal{X}_\alpha^2} \right)_{\lambda=0} \right| n, l \right\rangle. \quad (24)$$

The different factors included in the geometric perturbation,

$$\left(\frac{\partial \mathcal{J}_\alpha}{\partial \lambda} \right)_{\lambda=0}, \left(\frac{\partial^2 \mathcal{J}_\alpha}{\partial \lambda^2} \right)_{\lambda=0}, \frac{\partial}{\partial \lambda} \left(\frac{\mathcal{J}_\alpha}{\mathcal{X}_\alpha^2} \right)_{\lambda=0}, \frac{\partial^2}{\partial \lambda^2} \left(\frac{\mathcal{J}_\alpha}{\mathcal{X}_\alpha^2} \right)_{\lambda=0} \quad (25)$$

are also given in the Appendix. In the framework of the infinite confinement model, the parameter dependence of Eqs. (21)-(24) is known, since the matrix elements play the role of constants and need to be evaluated only once. Note also that the above expressions are not the same as those found in a typical perturbation theory, as the difference arising in the k^2 term depends on the perturbation Hamiltonian H_p , which itself depends on the parameter λ .

III. THE EIGENVALUES AND WAVEFUNCTIONS

Figure 2(a) shows the first 13 energy levels in units of $E_o = \hbar^2/(2m^*a^2)$ for a quantum lens calculated by perturbation theory up to the second order in $\lambda = \alpha^{-1} - 1$, as a function of

the ratio b/a . The different eigenvalue curves are labeled by the quantum numbers (N, m) . The semi-sphere case ($b/a = 1$) is indicated by the limiting value on the right vertical axis in each panel. One can see the breaking of degeneracy in the quantum number m , and the strong deviation from the semi-spherical case, as the ratio b/a decreases. The lower levels exhibit a weaker dependence on the decreasing b/a ratio, while the upper levels are strongly deviated from the semi-spherical case. In Fig. 2(b) the first 5 energy levels calculated up to first (dotted lines) and second order (solid lines) perturbation on the parameter λ are compared in the range $0.4 \leq b/a \leq 1$. It can be seen that a strong deviation is present for the higher excited levels ($N = 3$ and 4), while for $N = 1$ and 2 the obtained results using Eq. (23) (first order perturbation theory) give a deviation smaller than 1% in comparison with those using Eq. (24) (second order perturbation results).

The radial and angular probability density function in a given state N, m are defined as:

$$P_{N,m}(\rho) = \int_0^{\pi/2} |F_{N,m}(\rho, \theta)|^2 \rho \, d\theta, \quad P_{N,m}(\theta) = \int_0^a |F_{N,m}(\rho, \theta)|^2 \rho \, d\rho. \quad (26)$$

The functions $P(\rho)$ and $P(\theta)$ are obtained up to first order perturbation theory on λ according to the equations

$$P_{N,m}(\rho) = \rho \left(\frac{J_{l+1/2}(\mu_n^{(l)} \rho/a)}{N_B} \right)^2 \left[1 + \lambda \left(- \left\langle n, l \left| \left(\frac{\partial \mathcal{J}_\alpha}{\partial \lambda} \right)_{\lambda=0} \right| n, l \right\rangle + \int_0^{\pi/2} d\theta \sin \theta \left(\frac{\partial \mathcal{J}_\alpha}{\partial \lambda} \right)_{\lambda=0} \left(\frac{P_l^{(m)}(\cos \theta)}{N_{l,m}} \right)^2 \right] ; \rho \in (0, a) \quad (27)$$

and

$$P_{N,m}(\theta) = \sin \theta \left(\frac{P_l^{(m)}(\cos \theta)}{N_{l,m}} \right)^2 \left[1 + \lambda \left(- \left\langle n, l \left| \left(\frac{\partial \mathcal{J}_\alpha}{\partial \lambda} \right)_{\lambda=0} \right| n, l \right\rangle + \int_0^a d\rho \rho \left(\frac{\partial \mathcal{J}_\alpha}{\partial \lambda} \right)_{\lambda=0} \left(\frac{J_{l+1/2}(\mu_n^{(l)} \rho/a)}{N_B} \right)^2 \right] ; \theta \in (0, \pi/2). \quad (28)$$

Figure 3(a) and (b) show the radial and angular probabilities given by Eqs. (27) and (28), respectively. In both cases the levels considered are $(N, m) = (1, 0)$, $(4, 0)$, $(8, 0)$, and $(8, 2)$. Solid lines represent the semi-spherical case ($b/a = 1$), while the quantum cap with $b/a = 0.509$ is shown by dotted lines, and illustrates the departure from the semi-spherical case for decreasing b/a ratio. In the case of the radial probability, the deviation observed when the ratio b/a decreases is relatively small, in comparison with the semi-spherical cap. In contrast, the angular probability shows a rather strong deviation as a function of b/a , as the maximum probability is shifted towards $\theta = \pi/2$; that is, the carrier is located more towards the plane $v = 0$, as the cap height decreases (see Fig. 1(b)). For all states, the maximum of $P(\rho)$ is smoothly shifted towards $\rho = 0$, except for level $(8, 2)$. The different behavior observed for the radial and angular probability densities can be seen as arising from the fact that the geometry of the quantum dot is essentially decreasing in radius and not

in angle, as b/a decreases. The radial probability is obtained by integration along the angle in all directions ($0 < \theta < \pi/2$), taking into account the angular contribution for a given ρ and certain geometry. On the other hand, the angular probability is calculated by taking the integration along the radius where the change of geometry is more important. Hence, one can say that the angular probability density $P(\theta)$ contains more information about the changing cap geometry than the function $P(\rho)$, as function of b/a .

Finally, a test for the viability to obtain the wavefunctions and energies by the perturbation method, is given by the ratio between the matrix element of the perturbation Hamiltonian $\langle n, l | H_p(\mathcal{J}_\alpha, m) | n, l \rangle$ with respect to the non-perturbed dimensionless energy k_o^2 ,

$$\Delta_{N,m} \equiv \frac{|\langle n, l | H_p(\mathcal{J}_\alpha, m) | n, l \rangle|}{k_o^2(n, l)}. \quad (29)$$

The parameter $\Delta_{N,m}$ was calculated for the levels of Fig. 2 and is shown in Fig. 4 as a function of b/a . A necessary (but not sufficient) condition for the perturbation theory to be valid is that $\Delta_{N,m}$ must be less than the unity, and this criterion is fulfilled for the range $0.4 < b/a < 1$. Another more restrictive condition for the applicability of this method is that $\langle n, l | H_p(\mathcal{J}_\alpha, m) | n', l' \rangle < |k_o^2(n, l) - k_o^2(n', l')|$, saying that the differences between non-perturbed dimensionless energy states need to be larger than the matrix elements of the perturbation. A more complete, non-perturbation, solution of Eq. (7) is needed to completely assess the validity of the perturbation approach. However, one can be confident that for small λ values, the eigenstates and eigenfunctions found represent an accurate solution to the problem, as the perturbation and the small parameter is well defined, and the procedure robust.

IV. CONCLUSIONS

We have presented a formal and systematic conformal analytical map model to describe quantum dots with lens geometry and circular cross section arising in the growth of low dimensional semiconductor systems. The reported transformation can be extended straightforward to different physical-mathematical models as electronic states and phonon modes fulfilling a certain differential equation. The proposed conformal image maps the lens boundary into a dot with semi-spherical shape, allowing one to obtain a complete set of orthonormal functions to characterize the physical problem keeping the full lens symmetry. We have applied the formalism to the eigenvalue and eigenfunction of the Schrödinger problem in a spherical cap geometry. The conformal mapping of the equation allows a modified but well defined Rayleigh-Schrödinger perturbation approach, where the cap height to in-plane radius is used to define the small parameter of the theory.

We find that the wavefunctions are strongly shifted towards the flat face, as the height of the lens decreases, while the radial dependence is not affected as much. This change in the wavefunctions is interesting on its own, as it reflects the changes produced by the appropriate operator after the conformal mapping. Moreover, these changes may have important consequences for the different electronic and optical properties of self-assembled quantum dots. We are currently studying those properties and will report our findings in the future. The

reported energy dependence on cap height to in-plane radius and semiconductors parameters can be useful to characterize the geometrical dimensions of these novel semiconductor nanostructures.

ACKNOWLEDGMENTS

SEU acknowledges partial support by the US DOE grant no. DE-FG02-91ER45334.

APPENDIX

The Jacobian of the transformation $\mathcal{W}(\mathcal{Z})$ is given by

$$\mathcal{J}_\alpha(r, \theta) = \frac{16 (1/\alpha)^2}{R^{1-1/\alpha} [f_+^{1/\alpha} + f_-^{1/\alpha} + 2R^{1/2\alpha} \cos(\phi/\alpha)]^2}, \quad (\text{A1})$$

and the term $\mathcal{J}_\alpha/\mathcal{X}_\alpha^2$ can be cast as

$$\frac{\mathcal{J}_\alpha(r, \theta)}{\mathcal{X}_\alpha^2(r, \theta)} = \frac{16 (1/\alpha)^2}{R^{1-1/\alpha} [f_+^{1/\alpha} - f_-^{1/\alpha}]^2}. \quad (\text{A2})$$

In the above equations we have defined

$$r = \rho/a \quad ; \quad f_\pm = 1 + r^2 \pm 2r \sin \theta \quad ; \quad R = f_+ f_-, \quad (\text{A3})$$

and

$$\phi = \begin{cases} \arctg\left(\frac{2r \cos \theta}{1 - r^2}\right) & ; r < 1 \\ \pi/2 & ; r = 1 \end{cases}. \quad (\text{A4})$$

From Eqs. (A1) and (A2), it follows that

$$\mathcal{J}_{\alpha=1}(r, \theta) \equiv 1 ; \quad \left(\frac{\mathcal{J}_\alpha(r, \theta)}{\mathcal{X}_\alpha^2(r, \theta)} \right)_{\alpha=1} \equiv \frac{1}{r^2 \sin^2 \theta}, \quad (\text{A5})$$

as one would expect.

Finally, the geometric perturbation factors in Eq. (25) are given by

$$\left(\frac{\partial \mathcal{J}_\alpha(r, \theta)}{\partial \lambda} \right)_{\lambda=0} = 2 - r \sin \theta \ln(f_+/f_-) + 2\phi r \cos \theta, \quad (\text{A6})$$

$$\frac{\partial}{\partial \lambda} \left(\frac{\mathcal{J}_\alpha(r, \theta)}{\mathcal{X}_\alpha^2(r, \theta)} \right)_{\lambda=0} = \frac{4r \sin \theta - (1 + r^2) \ln(f_+/f_-)}{2r^3 \sin^3 \theta}, \quad (\text{A7})$$

$$\begin{aligned}
\left(\frac{\partial^2 \mathcal{J}_\alpha(r, \theta)}{\partial \lambda^2}\right)_{\lambda=0} &= \frac{1}{2} \left(\frac{\partial \mathcal{J}_\alpha}{\partial \lambda}\right)_{\lambda=0} \left[3 \left(\frac{\partial \mathcal{J}_\alpha}{\partial \lambda}\right)_{\lambda=0} - 8 \right] - \frac{(1+r^2)}{4} \ln^2(f_+/f_-) \\
&\quad + \phi^2(1-r^2) + 2 \ln^2 R,
\end{aligned} \tag{A8}$$

$$\begin{aligned}
\frac{\partial^2}{\partial \lambda^2} \left(\frac{\mathcal{J}_\alpha(r, \theta)}{\mathcal{X}_\alpha^2(r, \theta)} \right)_{\lambda=0} &= \frac{(4r \sin \theta)^2 - 16r \sin \theta (1+r^2) \ln(f_+/f_-)}{8r^4 \sin^4 \theta} \\
&\quad + \frac{(2(1+r^2)^2 + R) \ln^2(f_+/f_-)}{8r^4 \sin^4 \theta}.
\end{aligned} \tag{A9}$$

REFERENCES

- ¹ P.M. Petroff and G. Medeiros-Ribero, Mat. Res. Soc. Bull. **21**, 50 (April 1996).
- ² *Physics at Surfaces*, A. Zangwill (Cambridge University Press, 1988).
- ³ H. Lee, J.A. Johnson, J.S. Speck, and P.M. Petroff, Controlling ordering and positioning of InAs self-assembled quantum dots, preprint (March 2000).
- ⁴ D. Leonard, M. Krishnamurthy, C.M. Reaves, S. Denbaars, and P.M. Petroff, Appl. Phys. Lett. **63**, 3203 (1993); D. Leonard, K. Pond, and P.M. Petroff, Phys. Rev. B **50**, 11687 (1994).
- ⁵ S. Fafard, R. Leon, D. Leonard, J.L. Merz, and P.M. Petroff, Phys. Rev. B **50**, 8086 (1994).
- ⁶ J.-Y. Marzin, J.-M. Gerard, A. Izrael, D. Barrier, and G. Bastard, Phys. Rev. Lett. **73**, 716 (1994).
- ⁷ M. Grundmann, J. Christen, N.N. Ledentsov, J. Bohrer, D. Bimberg, S.S. Ruvimov, P. Werner, U. Richter, U. Gosele, J. Heydenreich, V.M. Ustinov, A. Yu. Egorov, A.E. Zhukov, P.S. Kop'ev, and Zh.I. Alferov, Phys. Rev. Lett. **74**, 4043 (1995).
- ⁸ R. Leon, P. M. Petroff, D. Leonard, and S. Fafard, Science **267**, 1966 (1995).
- ⁹ S. Lee, J.C. Kim, H. Rho, C.S. Kim, L.M. Smith, H.E. Jackson, J.K. Furdyna, M. Dobrowolska, Phys. Rev. B **61**, R2405 (2000).
- ¹⁰ H. Drexler, D. Leonard, W. Hansen, J.P. Kotthaus, and P.M. Petroff, Phys. Rev. Lett. **73**, 2252 (1994).
- ¹¹ M. Fricke, A. Lorke, J.P. Kotthaus, G. Medeiros-Ribeiro, and P.M. Petroff, Europhys. Lett. **36**, 197 (1996).
- ¹² G. Medeiros-Ribeiro, F.G. Pikus, P.M. Petroff, and A.L. Efros, Phys. Rev. B **55**, 1568 (1997).
- ¹³ A. Lorke, R.J. Luyken, A.O. Govorov, J.P. Kotthaus, J.M. Garcia, and P.M. Petroff, Phys. Rev. Lett. **84**, 2223 (2000).
- ¹⁴ B.T. Miller, W. Hansen, S. Manus, A. Lorke, and J.P. Kotthaus, Phys. Rev. B **56**, 6764 (1997).
- ¹⁵ T. Lundstrom, W.S. Schoenfeld, H. Lee, and P.M. Petroff, Science **286**, 2312 (1999).
- ¹⁶ M. Bayer, O. Stern, P. Hawrylak, S. Fafard, and A. Forchel, Nature **405**, 923 (2000).
- ¹⁷ See, for example, L.W. Wang, A.J. Williamson, A. Zunger, H. Jiang, and J. Singh, Appl. Phys. Lett. **76**, 339 (2000), and references therein.
- ¹⁸ R. J. Warburton, C. Schäfflein, D. Haft, F. Bickel, A. Lorke, K. Karrai, J. M. Garcia, W. Schoenfeld, and P. M. Petroff, Nature **405**, 926 (2000).

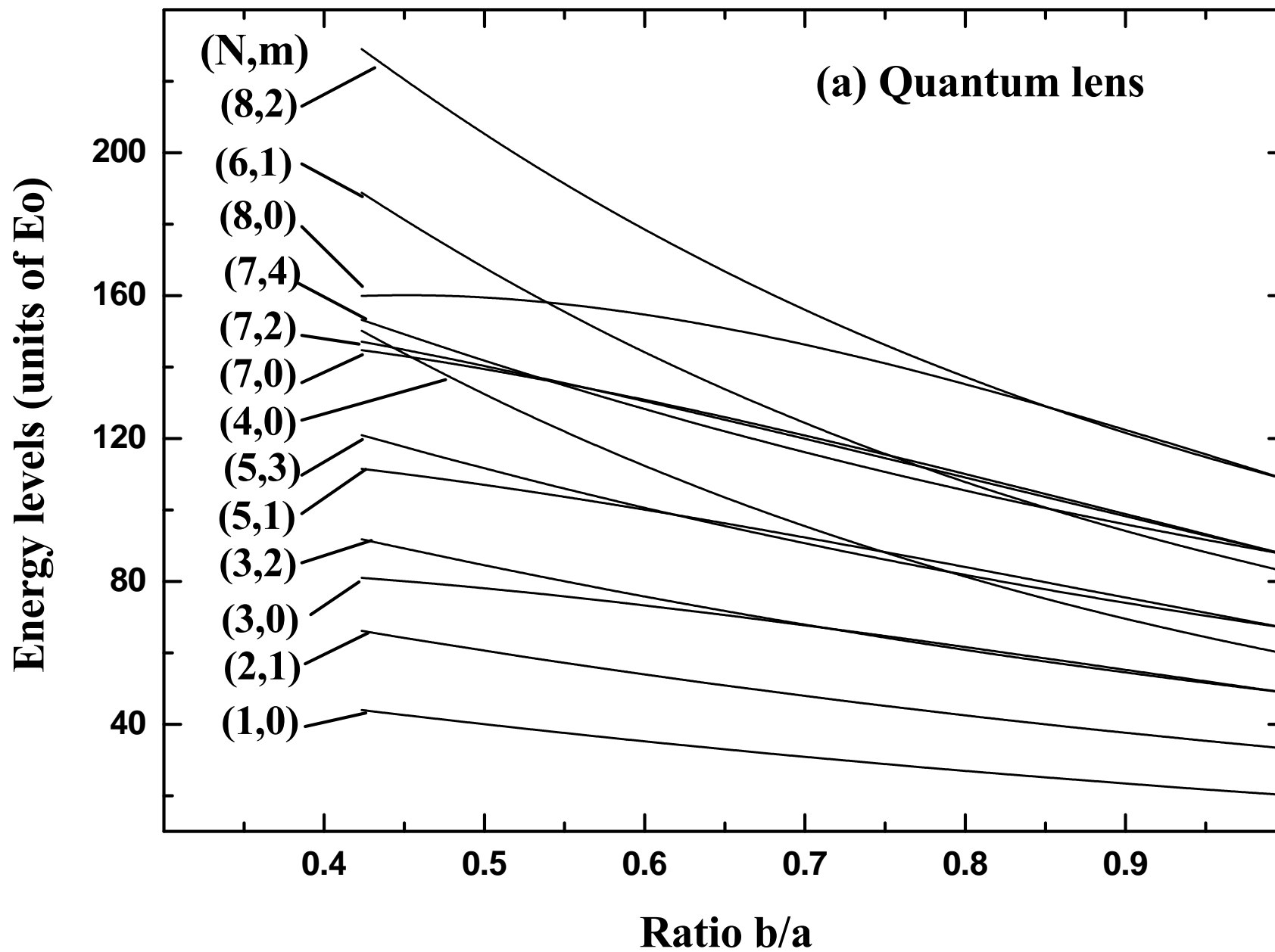
FIGURES

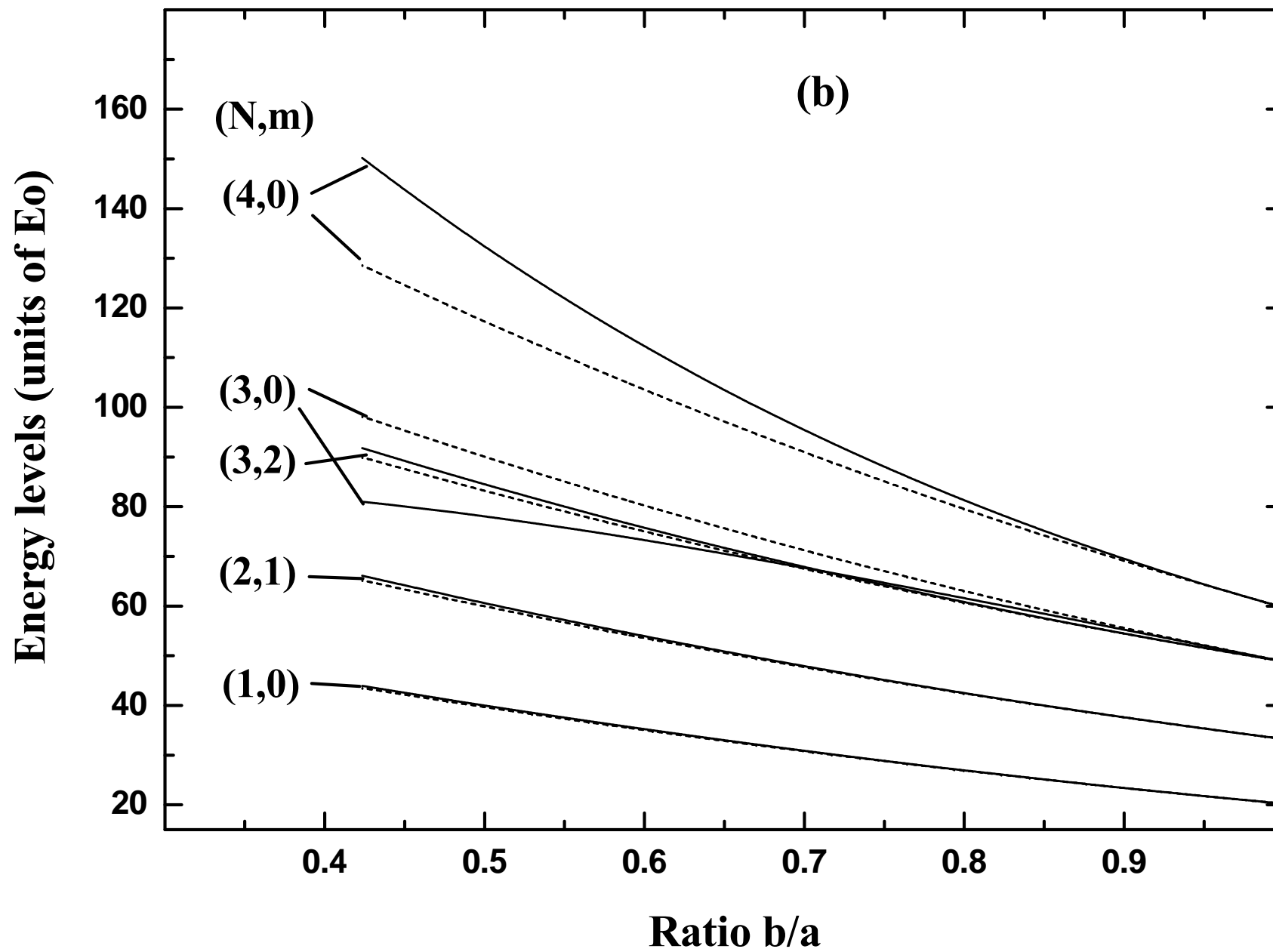
FIG. 1. (a) Lens cap of height b and radius a . (b) Conformal mapping from \mathcal{Z} to \mathcal{W} .

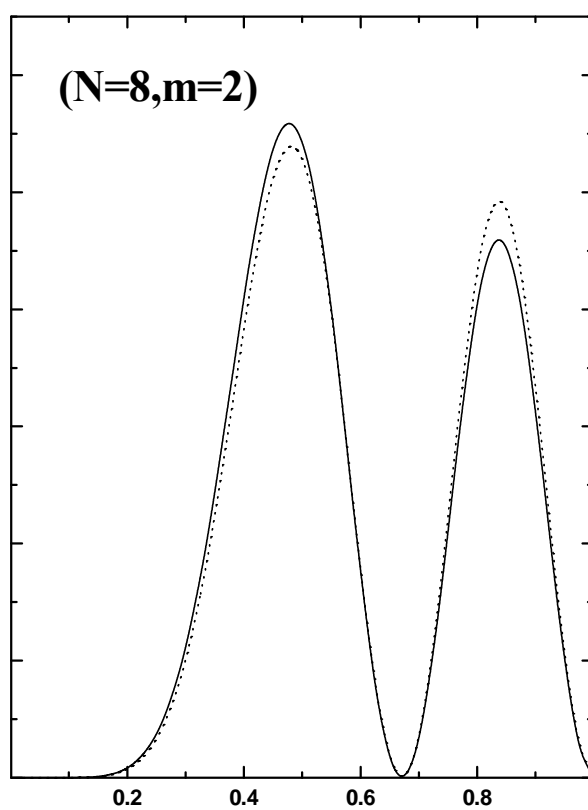
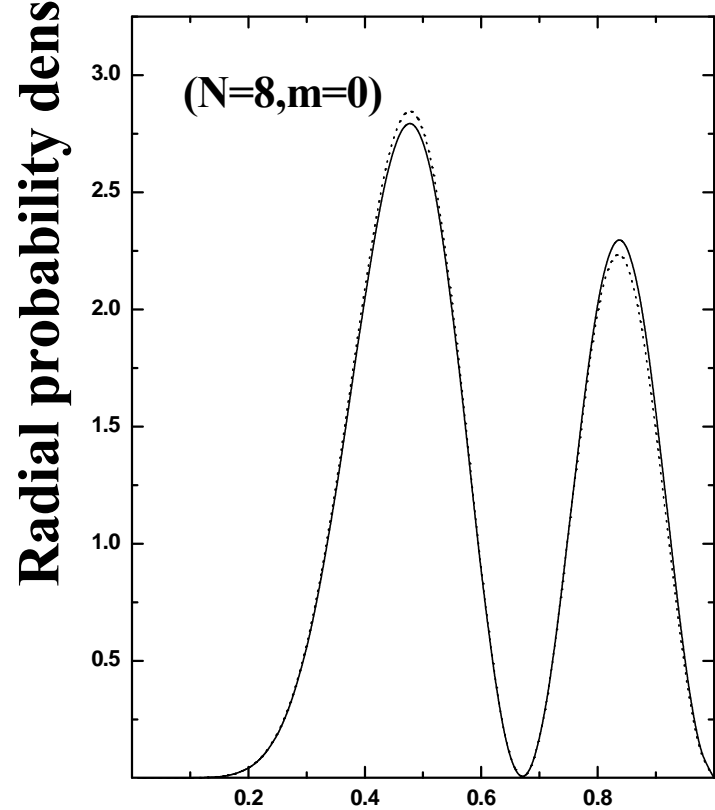
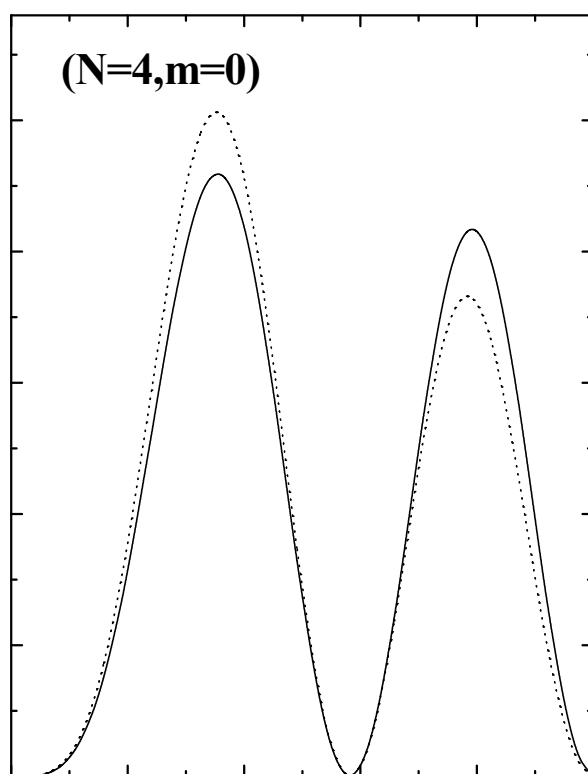
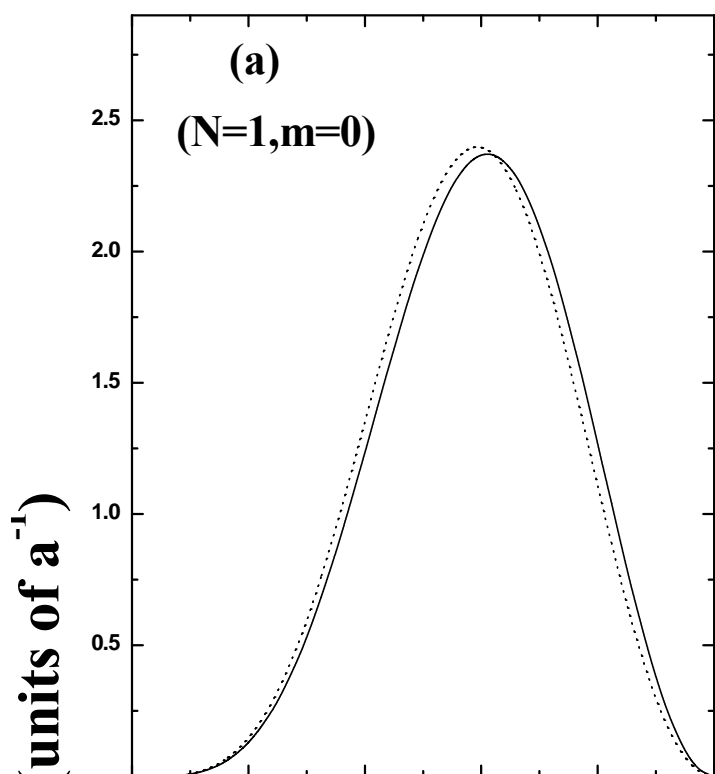
FIG. 2. Energy levels $E_{N,m}(b/a)$, labeled by (N, m) , for a quantum lens as a function of the ratio b/a . The energies are given in units of $E_0 = 2m^*E/\hbar^2$. (a) The first 13 energy levels calculated up to second order in perturbation theory. (b) Comparison between results calculated up to first (dotted lines) and second order (solid) perturbation theory for the first five levels.

FIG. 3. (a) The radial probability density in a quantum lens $P_{N,m}(\rho)$, in units of a^{-1} , for different electronic states (N, m) , and as function of the dimensionless coordinate $r = \rho/a$. (b) Angular probability density $P_{N,m}(\theta)$ as function of the angle θ . Two values of the ratio b/a are considered: $b/a = 1$ (solid lines), and $b/a = 0.509$ (dotted lines). The calculations were based on the perturbation theory described by Eqs. (27) and (28)). Different states $(N, m) = (1, 0)$, $(4, 0)$, $(8, 0)$, and $(8, 2)$ are indicated.

FIG. 4. Ratio between the matrix element Δ and the energy $k_o^2(n, l)$ with respect to the ratio b/a of the quantum lens. For all b/a between 0.4 and 1 the parameter Δ is small.



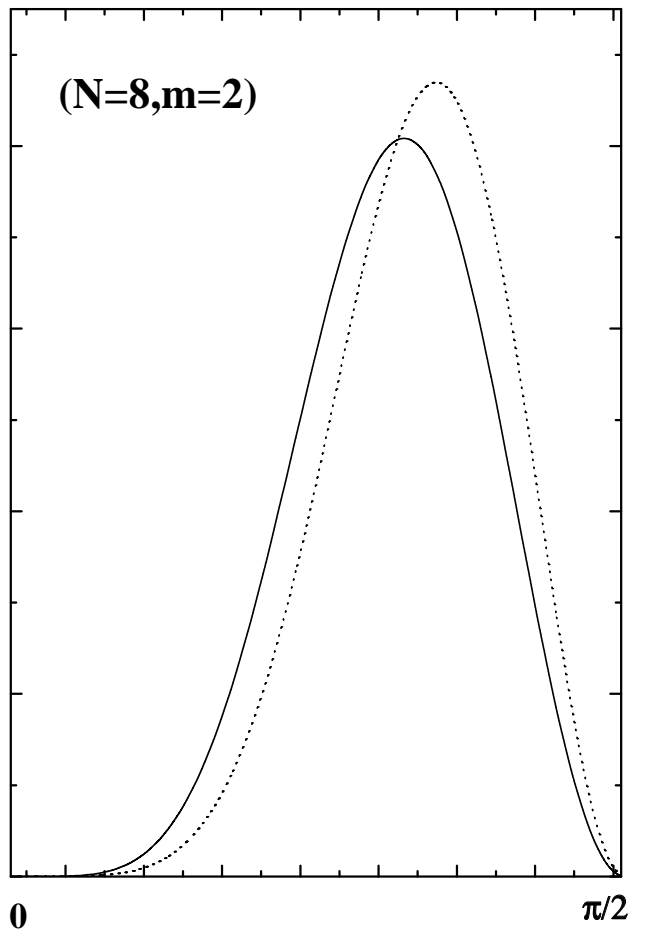
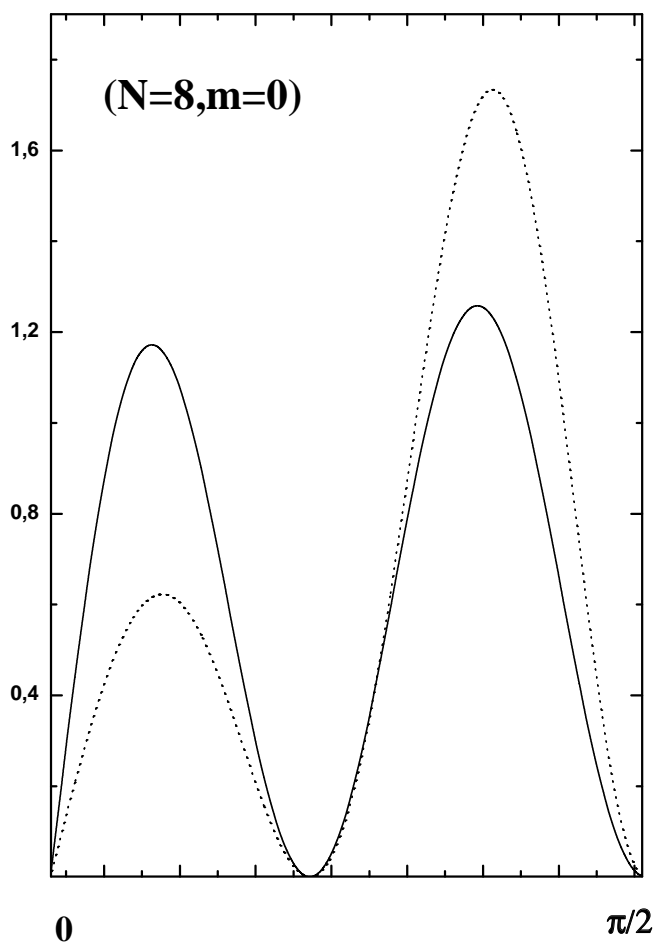
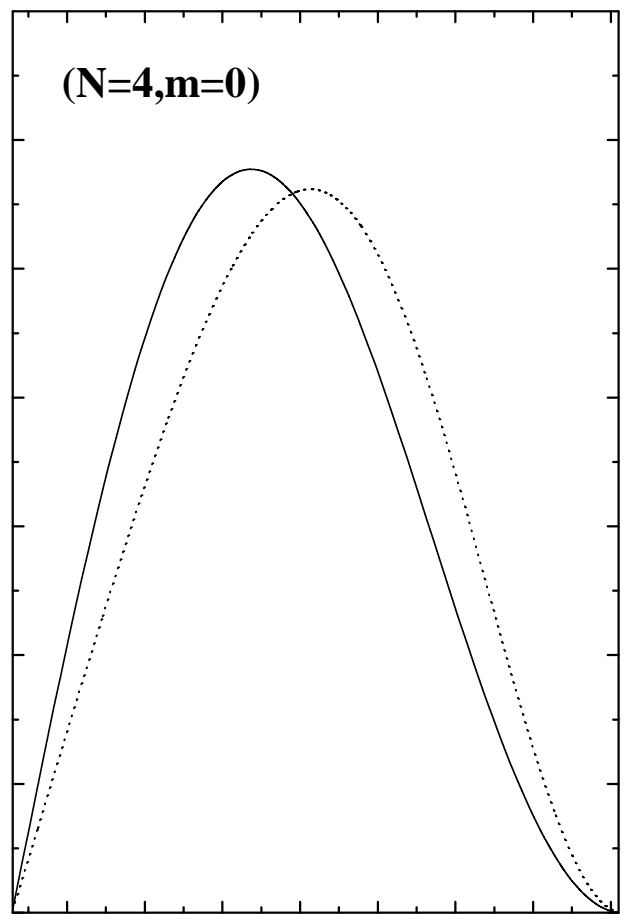
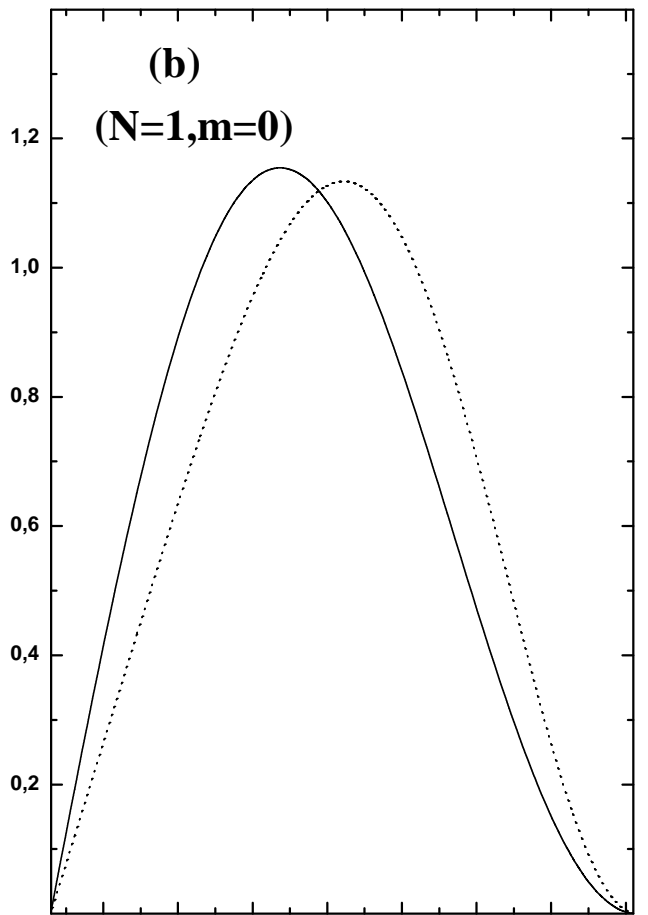




ρ/a

ρ/a

Angular Probab. Density



Angle(θ)

Angle(θ)

